ORIGINAL ARTICLE

Society For Biomaterials WILEY

Surface activation with oxygen plasma promotes osteogenesis with enhanced extracellular matrix formation in three-dimensional microporous scaffolds

Shuntaro Yamada[1] | Mohammed A. Yassin[1] | Tobias Weigel[2,3] |
Tobias Schmitz[2] | Jan Hansmann[2,3,4] | Kamal Mustafa[1]

[1]Department of Clinical Dentistry, Faculty of Medicine, University of Bergen, Bergen, Norway

[2]Chair of Tissue Engineering and Regenerative Medicine (TERM), University Hospital Würzburg, Würzburg, Germany

[3]Translational Center Regenerative Therapies, Fraunhofer Institute for Silicate Research (ISC), Würzburg, Germany

[4]Department Electrical Engineering, University for Applied Sciences Würzburg/Schweinfurt, Schweinfurt, Germany

Correspondence
Kamal Mustafa, Department of Clinical Dentistry, Faculty of Medicine, University of Bergen, Bergen, Norway.
Email: kamal.mustafa@uib.no

Abstract

Various types of synthetic polyesters have been developed as biomaterials for tissue engineering. These materials commonly possess biodegradability, biocompatibility, and formability, which are preferable properties for bone regeneration. The major challenge of using synthetic polyesters is the result of low cell affinity due to their hydrophobic nature, which hinders efficient cell seeding and active cell dynamics. To improve wettability, plasma treatment is widely used in industry. Here, we performed surface activation with oxygen plasma to hydrophobic copolymers, poly(L-lactide-co-trimethylene carbonate), which were shaped in 2D films and 3D microporous scaffolds, and then we evaluated the resulting surface properties and the cellular responses of rat bone marrow stem cells (rBMSC) to the material. Using scanning electron microscopy and Fourier-transform infrared spectroscopy, we demonstrated that short-term plasma treatment increased nanotopographical surface roughness and wettability with minimal change in surface chemistry. On treated surfaces, initial cell adhesion and elongation were significantly promoted, and seeding efficiency was improved. In an osteoinductive environment, rBMSC on plasma-treated scaffolds exhibited accelerated osteogenic differentiation with osteogenic markers including RUNX2, osterix, bone sialoprotein, and osteocalcin upregulated, and a greater amount of collagen matrix and mineral deposition were found. This study shows the utility of plasma surface activation for polymeric scaffolds in bone tissue engineering.

KEYWORDS
biomaterials, bone tissue engineering, lactide-TMC, mesenchymal stem cells, osteogenic differentiation, plasma activation

1 | INTRODUCTION

Calcified bone is a highly committed tissue where spontaneous healing and regeneration are severely limited after damage. This is a major challenge for modern medicine because complications related to bone are frequent as results of trauma, infection, and carcinoma. Current therapeutic approaches to patients with critical-sized bony defects include autologous, allogeneic and xenogeneic bone transplantation, the implantation of bioinert materials (e.g., titanium implants) and the use of synthetic biomaterial as bone substitutes, but

none of the treatments can achieve complete bone regeneration and functional recovery.[1,2] Meanwhile, a tissue engineering approach has been shown to be an alternative and promising means, which aims to regenerate functional tissues in combination with biomaterials, progenitor cells, and soluble factors.[3] This allows reducing therapeutic invasion to the patients, and it is theoretically applicable to defects in any size and shape. Biodegradable aliphatic polyesters have been developed as scaffolding materials in bone tissue engineering. Poly(L-lactide-co-trimethylene carbonate) (lactide-TMC) has been shown to be biocompatible to a greater or lesser degree depending on composition, allowing cellular events on the surface.[4-7]

For bone regeneration, biomaterials are preferably manufactured three-dimensionally with high porosity and interconnectivity to replicate bony structures in vivo.[8] However, the use of aliphatic polymers as three-dimensional (3D) microporous scaffolds is problematic because of their hydrophobic nature. Lactide-TMC, which is known to be more hydrophilic than first generation polyester biopolymers such as polylactic acid (PLA) and poly(ε-caprolactones) (PCL), is still not the exception.[6,9,10] Starting with cell seeding on the scaffolds, hydrophobicity hampers the infiltration of cell suspension into the micropores, which results in low seeding efficiency and inhomogeneous cell distribution.[11] This also causes the alteration of the "cell niche", leading to changes in paracrine signaling distance, cell-to-cell interaction and competitive nutrient supply.[12-16] Since the initial inhomogeneity persists, it may also mask or exaggerate cellular reactions to the environment. Therefore, various methods have been suggested as a means of surface modification such as chemical coating, alkaline hydrolysis, and plasma activation.[17]

Plasma activation is a surface modification procedure, which is widely used to hydrophilize material surfaces industrially. The effect is known to be attributed to the composition of polar functional groups (i.e., —OH, —COOH, —NH$_2$, —SO$_2$) on the materials and modification of nanotopography by etching and sputtering.[18] In regenerative medicine of bone tissue including orthoperiodic surgery and dentistry, the technique has been applied to promote faster healing and improve osteointegration of implanted devices, that is, titanium implant.[19] Recently, the application field has widened to the field of tissue engineering, and plasma activation of biodegradable aliphatic polyesters in combination with cells has become a focus of research. The effects of plasma activation using several different plasma sources (i.e., oxygen, nitrogen, argon, carbon dioxide, ammonia, and air plasma) has been tested using different cell types including vascular smooth muscle cells, umbilical endothelial cells, mammary epithelial cells, retinal pigment epithelial cells, keratinocytes, chondrocytes, osteoblasts, and fibroblast.[17,18] Based on these findings, it was recognized that appropriate plasma activation of polymeric scaffolds enhanced cellular adhesion by promoting the elongation of cell tentacles and proliferation although cells might behave differently depending on the type of cells and materials.[18,20] Osteoblastic cells, MC3T3-E1, responded to the plasma treated surface by upregulating their mRNA expression of alkaline phosphatase, osterix, runt-related transcription factor 2 (RUNX2), and osteocalcin.[21] This promotion of osteogenic property is suggested as a consequence of increased protein absorption on plasma-treated surfaces.[22] For multipotent cells, however, the effects of surface modification should not be restricted to proliferation and adhesion because physical surface properties are the key determinants of cell fate.[15,23] Indeed, several studies have suggested the change in nanotopography/hydrophilicity of the surfaces is responded by the alternation of multiple signaling pathways which are known to regulate cell fate. This includes $\alpha v\beta 1$ integrin signaling pathway,[24,25] Rho/Rock signaling pathway,[26] AP-1 signaling pathway[23] and canonical and non-canonical Wnt signaling pathways.[27,28] To date, comprehensive responses of multipotent cells on plasma-activated aliphatic polymers have not been well elucidated.

Thus, our aim was first to improve seeding efficiency by modifying the surface properties of 3D lactide-TMC scaffolds with oxygen plasma, and then, to explore the behaviors of rat bone marrow-derived stem cells (rBMSC) towards osteogenic differentiation. Here, we demonstrate that surface activation with oxygen plasma of two-dimensional (2D) films and 3D microporous scaffolds increased wettability mainly by roughening the surfaces nanoscopically. This consequently led to a notable improvement of seeding efficiency and allowed rBMSC to attach, elongate, and establish cell-to-cell interaction from an early phase of their growth. We further showed that it accelerated proliferative activity, extracellular matrix formation, and mineralization, with upregulation of lineage-specific markers for osteogenic differentiation. This study comprehensively evaluated adhesion, proliferation, and osteogenic differentiation of rBMSC in 3D microporous scaffolds treated with oxygen plasma for bone tissue engineering.

2 | MATERIALS AND METHODS

2.1 | Materials

The medical grade synthetic biomaterial lactide-TMC was purchased (RESOMER® LT706 S, Evonik) and used as a scaffold material as follows for this study.

2.2 | Methods

2.2.1 | Fabrication of 2D flat films and 3D microporous scaffolds of lactide-TMC

For 2D flat film preparation, lactide-TMC polymer was dissolved in chloroform and poured into glass petri dishes. After chloroform was completely evaporated, 10 mm diameter samples were punched out. For 3D microporous scaffold preparation, samples were prepared by a salt leaching technique.[29] Lactide-TMC polymer was dissolved in chloroform and then mixed with sodium chloride particles with a size range of 90–600 μm. After the complete evaporation of chloroform, scaffolds were prepared with a 10 mm diameter and 1.2 mm thickness. Subsequently, the scaffolds were thoroughly washed with distilled water to remove sodium chloride. Macro- and microstructures of the scaffolds and their topographical properties were evaluated by microCT (μCT) (see Figure A1 and Table 1, respectively).

	Average (*n* = 5)	SD
Weight (g)	0.012	0.0016
Thickness (mm)	1.22	0.084
Volume (mm^3)	95.82	6.57
Density (kg/m^3)	129.60	9.81
Porosity (%)	91.71	3.44
Open pores (%)	91.71	3.44
Close pores (%)	0.00031	0.00048

2.2.2 | Oxygen plasma activation and pre-treatment before cell seeding

The 2D flat films and 3D scaffolds were treated in a plasma chamber (Pico Plasma System, Diener electronics, Ebhausen, Germany) with oxygen plasma for 1, 3, or 5 min respectively, using a 100 kHz generator operated at a plasma process power of 350 W and pure oxygen gas (0.3 mbar, 12 sccm O_2).

For cell culture experiments, the treated-samples were placed in wells of low-adherent 48-well plates (10861–560; VWR International) and washed in 70% ethanol followed by through wash in PBS in sterile environment. The samples were then sterilized by ultraviolet (UV) radiation for 2 hr. The samples were then washed with PBS twice and pre-incubated in minimum of essential medium (αMEM) overnight before seeding.

2.2.3 | Fourier transform infrared spectroscopy (ATR-FTIR)

The ATR-FTIR spectra were recorded using an FT-IR-4100 instrument (Jasco, Gross-Umstadt, Germany). Each sample was measured by 128 scans and a resolution of 0.5 cm^{-1} in the range between 500 and 4000 cm^{-1}.

2.2.4 | Scanning electron microscopy

The samples were analyzed by scanning electron microscopy (SEM) using a high-resolution SEM (Zeiss CB 340, Oberkochen, Germany). Before SEM analysis, the samples were coated with a 2 nm coating of platinum in a sputter coater (EM ACE600, Leica, Vienna, Austria).

2.2.5 | Contact angle measurement and 3D hydrophilic assessment

Surface wettability of the 2D flat films was determined with a contact angle measuring device (OCA 15EC, Dataphysics, Filderstadt,

Germany) using 3 μl of ultrapure water dripped onto the surface. The experiment was performed on three different samples for each condition (0, 1, 3, 5 min of plasma treatment). In order to evaluate the treatment's stability over time, the measurements were repeated on fresh samples 2 weeks after the plasma process.

For wettability evaluation of the 3D microporous scaffolds, the measurement took place 2 weeks after the plasma activation. 50 μl αMEM was dropped on each scaffold. Photographic images were captured after 60 s.

2.2.6 | Cell culture and seeding

The study was approved by the Norwegian Animal Research Authority and performed according to the European Convention for the Protection of Vertebrates used for Scientific Purposes (local approval number 20146866). Bone marrow stem cells were isolated from the femurs of Lewis rats (rBMSC) as previously described[30] and maintained in αMEM supplemented with 10% fetal bovine serum (FBS) and 1% penicillin–streptomycin at 37°C in 5% CO_2 humidified atmosphere. Cells from passage 3–4 were used for the study. When the cells reached approximately 80% confluence, the cells were trypsinized, and 10,000 and 100,000 cells were seeded on the lactide-TMC films and the microporous scaffolds in the 48 well plates, respectively. After seeding, the well plates were stirred at 800 rpm for 30 s to homogenize cell distribution. Flat films were collected 24 hr after seeding. For the evaluation of osteogenesis of rBMSC, the 3D microporous scaffolds that were treated with oxygen plasma for 3 min were transferred into osteoinductive medium, αMEM supplemented with 200 nM dexamethasone, 10 mM glycerophosphate and 0.05 mM ascorbic acid on the following day (day 0) and evaluated on days 1, 3, 7, 14, and 21. The experimental timeline is shown in Figure A2.

2.2.7 | Evaluation of seeding efficiency and viability

3D microporous scaffolds were used for the evaluation of seeding efficiency. Three hours after seeding, non-adherent cells and cells attached on wells, not scaffolds, were collected and stained with 0.4% Trypan blue solution (T10282; Invitrogen). The number of cells and viability was counted using a Countess Automated Cell Counter (A27977; Invitrogen). Seeding efficiency was calculated as follows:

$$\text{Seeding efficiency} (\%) = 1 - \frac{\text{Cells left in a well} + \text{Non adherent cells}}{\text{Cells seeded on a scaffold}}$$

2.2.8 | Immunofluorescence and image analyses

2D film samples and 3D microporous scaffolds for immunofluorescence were collected 3, 6, and 24 hr after seeding and day 3, 7, 14, and 21, respectively. Samples for F-actin, RUNX2, and PCNA staining were fixed in 4% paraformaldehyde for 15 min at room

temperature, and samples for Col1 and β-Actin staining were fixed in cold methanol for 10 min. For PCNA staining only, antigen retrieval was performed with 10 mM sodium citrate (pH 6) at 95°C for 20 min. The samples were then permeabilized in 0.1% Triton X-100 in PBS (PBST) for 10 min three times and blocked with 10% goat serum in PBST for 1 hr at room temperature followed by incubation with primary antibodies at 4°C overnight. Primary antibodies used were as follows: anti-collagen I antibody (1:1000, ab90395; Abcam, UK), anti-Runx2 antibody (1:250, ab23981; Abcam, UK), anti-β-Actin antibody (1:100, PA1-183; Thermo Fisher Scientific), anti-PCNA antibody (1:200, sc-56; Santa Cruz). After washes in PBS 6 times (10 min each), the samples were incubated for 1 hr at room temperature with species-specific secondary antibodies conjugated to AlexaFluor 488/568/635 (1:250, A11008/A11011/A31575; Life Technology). Nuclei and F-actin (for RUNX2 staining only) were counterstained with 4′,6-diamidino-2-phenylindole (DAPI; 1:5000, 62,247; Thermo Fisher Scientific) and Alexa Fluor 488 Phalloidin (1:500, A12379; Invitrogen), respectively. Specimens were washed six times (10 min each) with PBST and mounted on confocal dishes in PBS. Stack images with a z-step size of 0.8 μm were acquired by a confocal microscope (TCS SP8; Leica, Germany) with a water immersion 25× objective. Images were obtained by the same acquisition setting, and each channel was separately obtained by a sequential scan function to perform quantitative analyses. Images were processed in Fiji/ImageJ for quantification.[31]

2.2.9 | Double-strand DNA quantification

Samples were collected on days 1, 3, 7, 14, and 21 and immersed in PBST following a wash with PBS. Freezing–thawing cycle at −80°C was repeated twice to collect cytolysate from the samples. Double strand DNA (dsDNA) was quantified by using Quant-iT™ PicoGreen™ dsDNA Assay Kit (P7589; Invitrogen) according to the manufactures

TABLE 2 Primers used for RT-qPCR gene expression analysis

Gene	Symbol	Cat. No.
Glyceraldehyde-3-phosphate dehydrogenase	GAPDH	Rn01749022_g1
Runt-related transcription factor 2	RUNX2	Rn01512298_m1
Collagen, type I, alpha 1	Col1A1	Rn01463848_m1
Alkaline phosphatase	ALP	Rn01516028_m1
Bone sialoprotein	BSP	Rn00561414_m1
Sp7 transcription factor	Sp7 (Osterix)	Rn01761789_m1
Bone gamma-carboxyglutamate protein	Bglap (Osteocalcin: OCN)	Rn00566386_g1
Thy-1	Thy1 (CD90)	Rn00562048_m1
Ecto-5′-nucleotidase	Nt5e (CD73)	Rn00665212_m1
CD44	CD44	Rn00681157_m1

protocol. Fluorescence intensity was measured with an excitation wavelength of 480 nm and emission wavelength of 520 nm using Varioskan™ LUX multimode microplate reader (VLBL00D0; Thermo Fisher Scientific, Finland).

2.2.10 | Total RNA extraction and reverse transcription polymerase chain reaction

Samples for RT-qPCR were collected on days 3, 7, 14, and 21. RNA extraction was performed using a Maxwell® 16 Cell LEV Total RNA Purification Kit (AS1280; Promega) in accordance with protocol provided by the supplier. Reverse transcription was then performed with the High Capacity cDNA Reverse Transcription Kit (4,368,814; Applied Biosystems). RT-qPCR was performed on StepOne™ Real-Time PCR System with T TaqMan™ Gene Expression Assay (4,453,320, Applied Biosystems). Primers used are given in Table 2. The amplification was performed as follow: initial denaturation at 95°C for 20 s, followed by 40 cycles of 95°C for 1 s and 60°C for 20 s. Each sample was assessed in triplicate. Specificity of the reaction was assessed by amplification curve, and the relative expression of the genes was calculated using the $2^{-\Delta\Delta CT}$ method following to normalization to a housekeeping gene GAPDH.[32]

2.2.11 | Alkaline phosphatase activity assay

Samples were collected on days 1, 3, 7, 14, and 21. Cytolysate was collected by freezing–thawing cycle at −80°C, equal volume of P-nitrophenyl phosphate (pNPP, 20–106; Sigma-Aldrich, Germany) was added in each sample. Absorbance was measured at 405 nm using a Varioskan™ LUX multimode microplate reader (VLBL00D0; Thermo Fisher Scientific, Finland).

2.2.12 | Alizarin red S staining and quantification

Samples taken on days 1, 3, 7, 14, and 21 were fixed in 4% PFA for 40 min and washed three times with Milli-Q® water. The samples were then incubated with 0.1% Alizarin Red S for 20 min followed by thorough wash with Milli-Q® water. For quantification, the dye was extracted with 100 mM cetylpyridium chloride overnight. Absorbance of the extract was measured at 540 nm using a Varioskan™ LUX multimode microplate reader (VLBL00D0; Thermo Fisher Scientific, Finland).
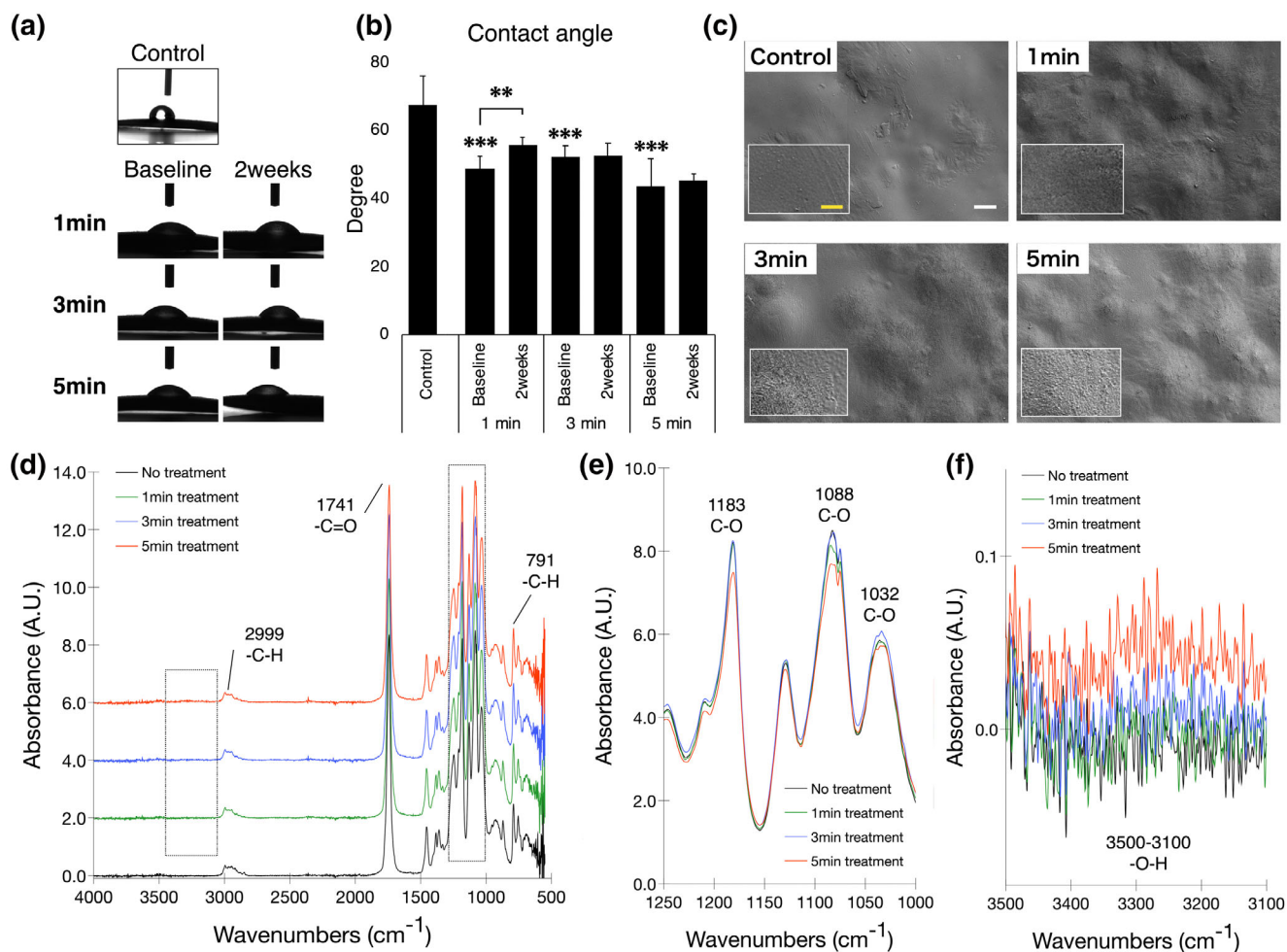
2.2.13 | Statistics

All statistical analyses were conducted with SPSS 24.0 (IBM). For the comparison of 1, 3, and 5 min-treated groups to the control, one-way ANOVA followed by Dunnett post hoc test was performed. Pairwise comparison was performed by Student's t test. For RT-qPCR, logarithmic value of $2^{-\Delta\Delta CT}$ was calculated to normalize to the endogenous

FIGURE 1 Surface characterization before and after plasma activation with oxygen of 2D films of lactide-TMC. (a,b) Water contact angle measurement before, immediately after and 2 weeks after plasma activation for 1, 3, and 5 min. Values are presented as mean ± SD. *$p < .05$, **$p < .01$, ***$p < .001$. (c) Scanning electron microscopy images of plasma-treated 2D films. Scale bar: white = 10 μm, yellow = 1 μm. (d) Offset ATR-FTIR spectrum of plasma-treated films. (e) Super-positioned ATR-FTIR spectrum between 1250 and 1000 cm^{-1} indicating an ether group (—C—O) and (f) 3500 and 3100 cm^{-1} indicating an alcohol group (—O—H)

control and evaluated by Student's *t* test. $p < .05$ was considered statistically significant.

3 | RESULTS

3.1 | Plasma activation with oxygen plasma hydrophilized lactide-TMC by roughening the surfaces nanotopographically with a slight increase in an alcohol group

Lactide-TMC films were plasma-treated for 1, 3, and 5 min, and the contact angle was significantly reduced by approximately 20–25° in all groups ($p < .001$). The effect was maintained for at least 2 weeks except for one treated for 1 min in which the recurrence was observed ($p = .006$) (Figure 1(a,b)). SEM revealed that the surfaces were spotted in plasma-treated groups, and the level of nano-roughness was correlated with the dosage of oxygen plasma (Figure 1

(c)). Surface chemistry was evaluated by ATR-FTIR spectra, showing that there was a minimum change in chemical composition before and after the treatment. Characteristic peaks were observed at 2999, 1741, 1183–1032, and 791 cm^{-1}, which are assigned to —C—H, —C=O, —C—O, and —C—H, respectively. These peaks were almost identical among the groups except for the 5 min-treated samples in which the intensity of —C—O decreased (Figure 1(d,e)). In the range between 3500 and 3100 cm^{-1}, which is assigned to —O—H group, the absorbance slightly increased in the plasma-treated groups in a dose-dependent manner (Figure 1(f)).

3.2 | Plasma-treated surfaces promote initial adhesion, elongation, and proliferation of rBMSC

To access the initial cellular adhesion, elongation and proliferation, rBMSC were seeded on flat films treated with oxygen plasma. After 3–6 hr of seeding, cells attached on plasma-treated films exhibited
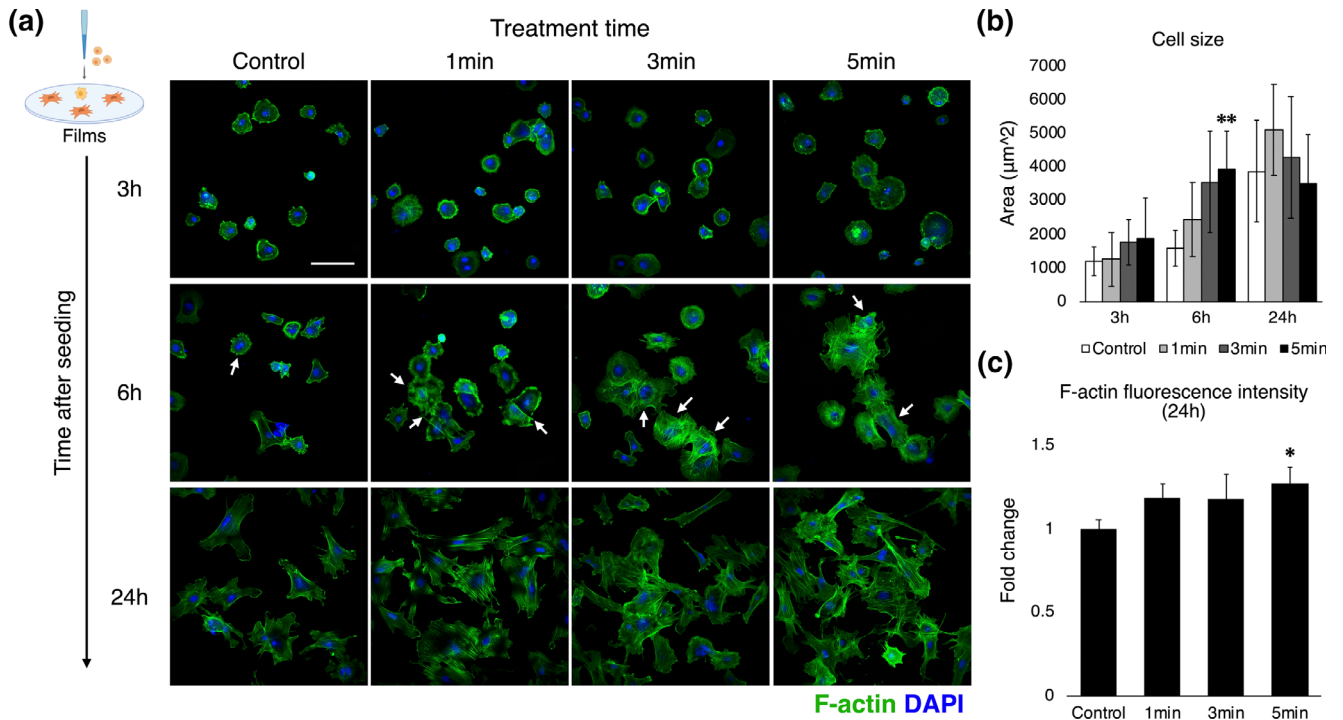
FIGURE 2 Initial cell adhesion, elongation, and proliferation on the plasma-treated 2D films. (a) Confocal images of bone marrow stem cells stained for F-actin and nuclei after 3, 6, and 24 hr of cell seeding on plasma-treated films. Arrows indicate cells undergoing cell divisions. (b) the image quantification of cell size and (c) F-actin fluorescence intensity measured at 24 hr of seeding. Values are presented as mean ± SD. Scale bar = 100 μm. *$p < .05$, **$p < .01$

more extended morphology than on the control despite the heterogeneous cell population causing large variation in the morphological quantification. Notably, active cellular proliferation and elongation were clearly observed on plasma-treated films at 6 hr, which resulted in the formation of complex cell-to-cell interaction. This also led to the stagnation or reduction in cell size in the 3 and 5 min-treated groups at 24 hr because of high cell density. On the other hand, cells on the control surface were less elongated, remaining isolated over the time (Figure 2(a,b)). There was a tendency for an increase in F-actin intensity in longer plasma-treated groups, indicating enhanced actin polymerization on the plasma-treated surfaces ($p = .026$ between the control and the 5 min-treated group) (Figure 2(c)).

3.3 | Improvement of hydrophilicity and seeding efficiency on 3D LTMC scaffolds

3D microporous scaffolds were treated with oxygen plasma for 1, 3, and 5 min to improve surface hydrophilicity without altering macro/micro-structure of the scaffolds. After the drop of αMEM, the medium almost immediately soaked into the scaffolds treated for more than 3 min while the droplet maintained an elliptical shape on the control and 1 min-treated scaffolds (Figure 3(a)). As with the 2D films, the surfaces were roughened with the texture of nanoscopic spots by oxygen plasma, which was limited superficially in submicron scale (Figure 3 (b)). Consistent with wettability, cell seeding efficiency was

significantly improved in the groups treated for 3 and 5 min compared to the control ($p = .027$ and .016, respectively) (Figure 3(c)). It is noteworthy that, due to the low absorbency, medium was distributed unevenly within the control scaffolds. However, prolonged plasma treatment negatively correlated with cell viability for the cells that remained on the wells, particularly in the 5 min-treated group ($p = .006$) (Figure 3(d)).

3.4 | Increase in cellular proliferation on plasma-treated scaffolds

rBMSC were seeded on control and plasma-treated scaffolds for 3 min, and cellular proliferation was evaluated on days 1, 3, 7, 14, and 21 after seeding. The quantification of dsDNA shows statistical significance between the control and plasma-treated scaffolds on day 1 ($p = .049$) and day 3 ($p = .007$), and proliferative activity reached the highest level in both groups around day 7. Subsequently, suppression of proliferation was observed in both groups. While the control group showed a gradual decrease by day 21, proliferative activity of cells on the plasma-treated scaffolds had already nadired on day 14 ($p = .0014$) (Figure 4(a)). To assess cell cycle status, samples were stained with anti-PCNA antibody. After seeding, the majority of cells in both groups expressed PCNA, indicating the cells were proliferative. Cells highly expressing PCNA (PCNA[High+] cells) accounted for the majority of cells by day 7, but

(a)

(b)

(c)

(d)
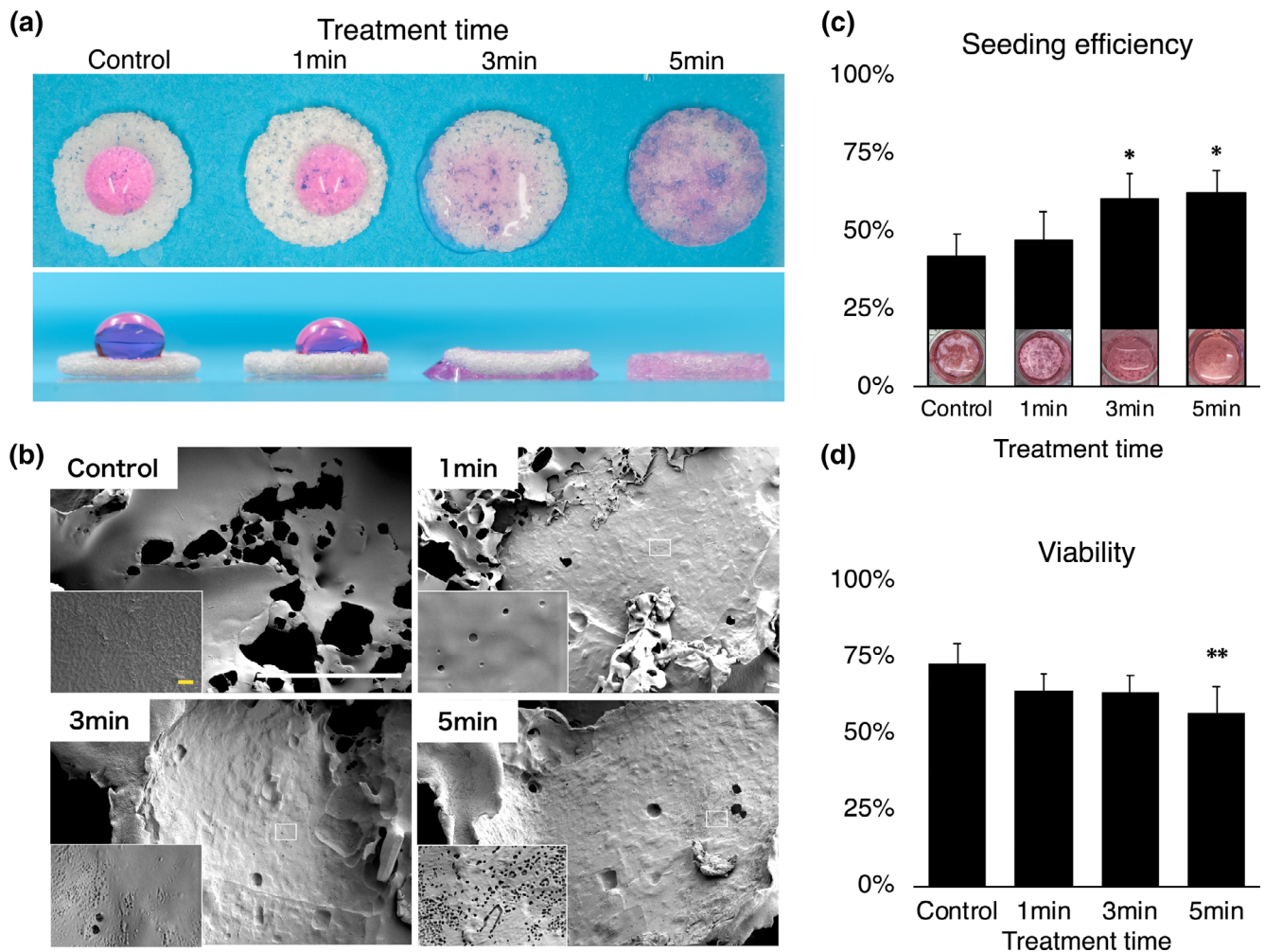
FIGURE 3 Characterization of surface topography and measurement of seeding efficiency with 3D microporous lactide-TMC scaffolds after plasma activation with oxygen plasma. (a) Photographical images of medium droplets on microporous scaffolds treated with oxygen plasma for 1, 3, and 5 min. The images were taken at 60 s of a drop of 50 μl α-MEM. (b) Scanning electron microscopy images of plasma-treated 3D microporous scaffolds. The magnified parts were marked with white boxes. Scale bar: white = 100 μm, yellow = 1 μm. (c) Seeding efficiency with the representative appearance of the scaffolds in wells and (d) cell viability measured after 1 hr of seeding. Values are presented as mean ± SD. *$p < .05$, **$p < .01$

PCNA expression was downregulated afterwards, and cells weakly expressing PCNA (PCNA^{low+} cells) became the majority on day14 and 21 (Figure 4(b)). Quantification shows that approximately 70% of the cells expressed PCNA by day14 in both groups, slightly higher in the plasma-treated group, after which proliferation was significantly down regulated (Figure 4(c)).

3.5 | Promotion of osteogenic differentiation on plasma-treated scaffolds

To evaluate osteogenic differentiation, mRNA expression of osteogenic markers, RUNX2, Col1A1, bone sialoprotein (BSP), osterix, ALP, and OCN was measured (Figure 5(a)). A key transcription factor and early osteogenic marker, RUNX2, remained upregulated by day 14 in both groups. The cells on plasma-treated scaffolds showed significant upregulation of RUNX2 on day 7 ($p = .015$) compared with rBMSC on

control scaffolds. The peak was observed on day 14 in the control group while the RUNX2 level was stable from day 14 to day 21 in the plasma-treated group. The expression of an early osteogenic marker, Col1A1, was significantly upregulated as early as day 3 in the plasma-treated group ($p = .042$), which was the highest throughout the experimental period. The peak of ColA1 expression in the control group was observed on day 7 ($p = .0044$). Another osteogenic marker, ALP, displayed continuous upregulation over time in both groups. However, regarding the comparison between groups, the regulatory pattern was time-dependant and did not show a clear pattern. The expression of osterix, an osteogenic marker related to the maturation process of pre-osteoblasts, increased continuously over time in both groups. Notably, the plasma-treated group consistently showed higher expression compared with the control (day 7 $p = .006$, day 21 $p = .008$). Similarly, BSP was significantly upregulated on day 3 and day 21 in the plasma-treated group (day 3 $p = .00089$, day 21 $p = .028$).[33] A late osteogenic marker, OCN, clearly indicated that the

(a)

(b) Control   PCNA DAPI   Plasma-treated

(c)
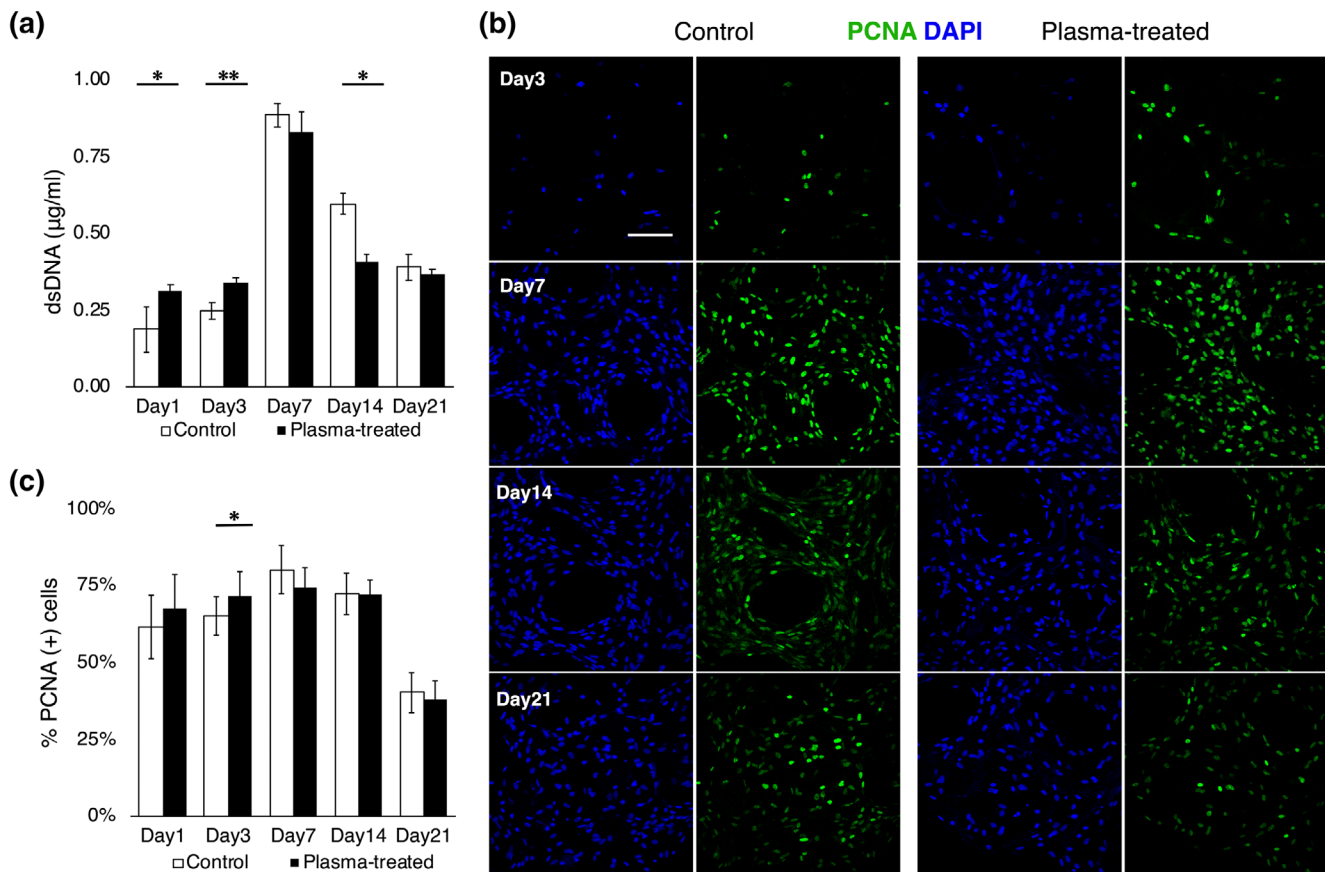
FIGURE 4 Proliferative activity and cell cycle of bone marrow stem cells on the 3D plasma-treated scaffolds for 3 min. (a) The quantification of dsDNA of bone marrow stem cells on day 1, 3, 7, 14, and 21 after seeding. (b) Immunofluorescence images for PCNA on day 3, 7, 14, and 21 after seeding. Scale bar = 100 μm. (c) The image quantification of the ratio of PCNA positive cells. Values are presented as mean ± *SD*. *$p < .05$, **$p < .01$

expression was enhanced in the late stage, particularly in the plasma-treated group, and a significant difference between the groups was observed on day 14 ($p = .047$) and day 21 ($p = .020$). To evaluate the general property as MSC, putative markers for rat MSC, CD44, CD73, and CD90, were measured.[34] These were expressed consistently with a small fluctuation throughout the experimental period, following a comparable tendency in both groups (Figure 5(b)).

Immunofluorescence showed that RUNX was highly expressed throughout the experiment in both groups (Figure 5(c)). The nuclear accumulation of RUNX2 was found mainly on day 7 and day 14, and the expression was diffused to cytoplasm on day 21. This indicates that the early RUNX2 expression acted as a transcription factor for osteogenic differentiation. Notably, the groups of cells with RUNX2 highly expressed in nuclei were focally found on day 7 only in the plasma-treated group.

3.6 | Accelerated differentiation confirmed by the increased level of collagen matrix formation

To evaluate the formation of extracellular matrix, samples were stained with anti-collagen I antibody which specifically reacts with non-denaturing 3D helical structure of native collagen type I (Col1).

Consistent with the early expression of osteogenic markers, collagen formation was significantly accelerated on plasma-treated scaffolds (Figure 6(a)). While the Col1 formation gradually increased over time in the control group, the remarkable Col1 formation was observed as early as 7 days post-osteoinduction in the plasma-treated group. Quantification of surface coverage by Col1 shows that it reached approximately 50% on day 7 in the plasma-treated group, which was 20% higher than the control ($p = .037$) (Figure 6(b)). On day 21, the control group caught up to the plasma-treated group. Col1 intensity was slightly higher in the plasma-treated group on day 7 and day 21, suggesting the formation of a dense Col1 layer, but it was not statistically significant (Figure 6(c)).

3.7 | Enhanced mineralization on plasma-treated scaffolds

To assess mineralization as a consequence of osteogenic differentiation, ALP activity and calcium deposition were evaluated. ALP activity was continuously upregulated by day 14 in both groups (Figure 7(a)). Although the upregulation of ALP activity in the plasma-treated group was found on day 1 and day 3, the increase ratio over time was lower. Alizarin red S quantification showed the promotion of mineralization
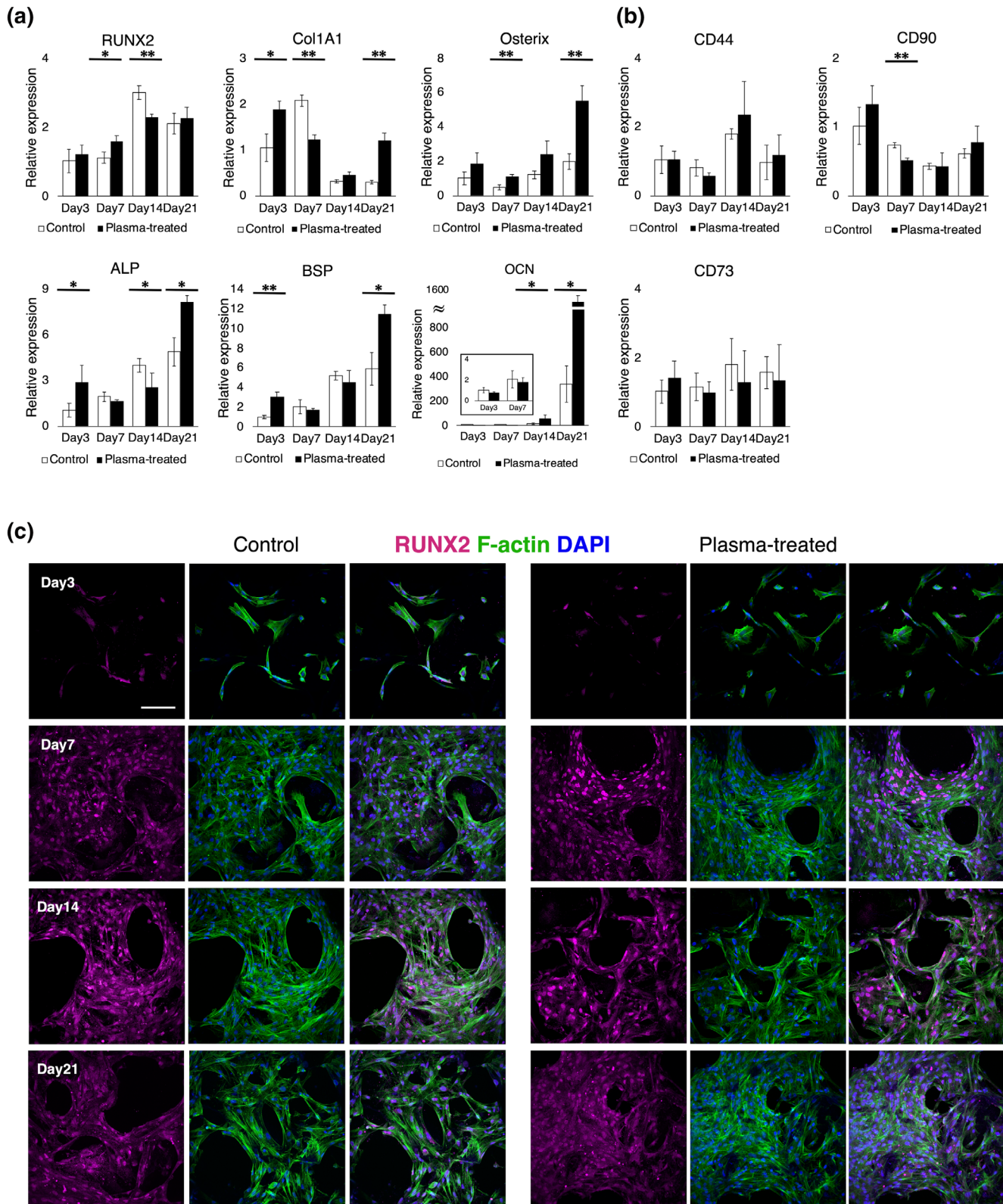
FIGURE 5 Evaluation of osteogenic differentiation of bone marrow stem cells on the 3D plasma-treated scaffolds for 3 min. (a,b) mRNA expression of osteogenic differentiation markers and a putative mesenchymal stem cell marker on day 3, 7, 14, and 21 after seeding on the 3D plasma-treated scaffolds. Relative mRNA levels were normalized to GAPDH. Values are presented as mean ± 95% confidence interval. *$p < .05$, **$p < .01$, ***$p < .001$ (c) immunofluorescence images for RUNX2. Scale bar = 100 μm

in the plasma-treated group (Figure 7(b,c)). Interestingly, calcium deposition in the control was not as homogeneous as their counter-part on day 7, demonstrating the heterogeneity of cell distribution.

Quantification confirmed the greater production of calcium by cells on plasma-treated scaffolds, particularly on day 3 ($p = .031$) and day 7 ($p = .003$) (Figure 7(d)).
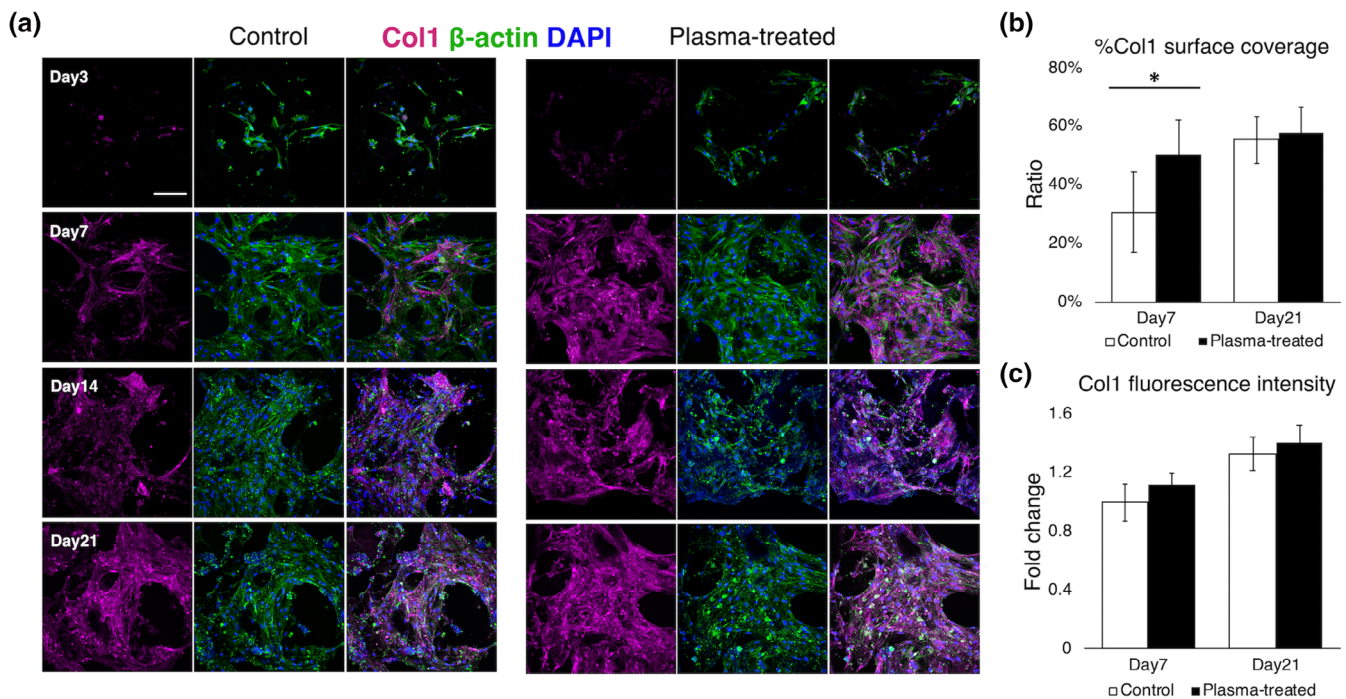
FIGURE 6 Collagen type 1 formation by bone marrow stem cells on the 3D plasma-treated scaffolds for 3 min. (a) Immunofluorescence images for collagen type 1 on day 3, 7, 14, and 21 after seeding. Scale bar = 100 μm. The quantifications of (b) surface coverage rate and (c) fluorescence intensity of collagen type 1 on day 7 and day 21 after seeding. Values are presented as mean ± *SD*. *$p < .05$
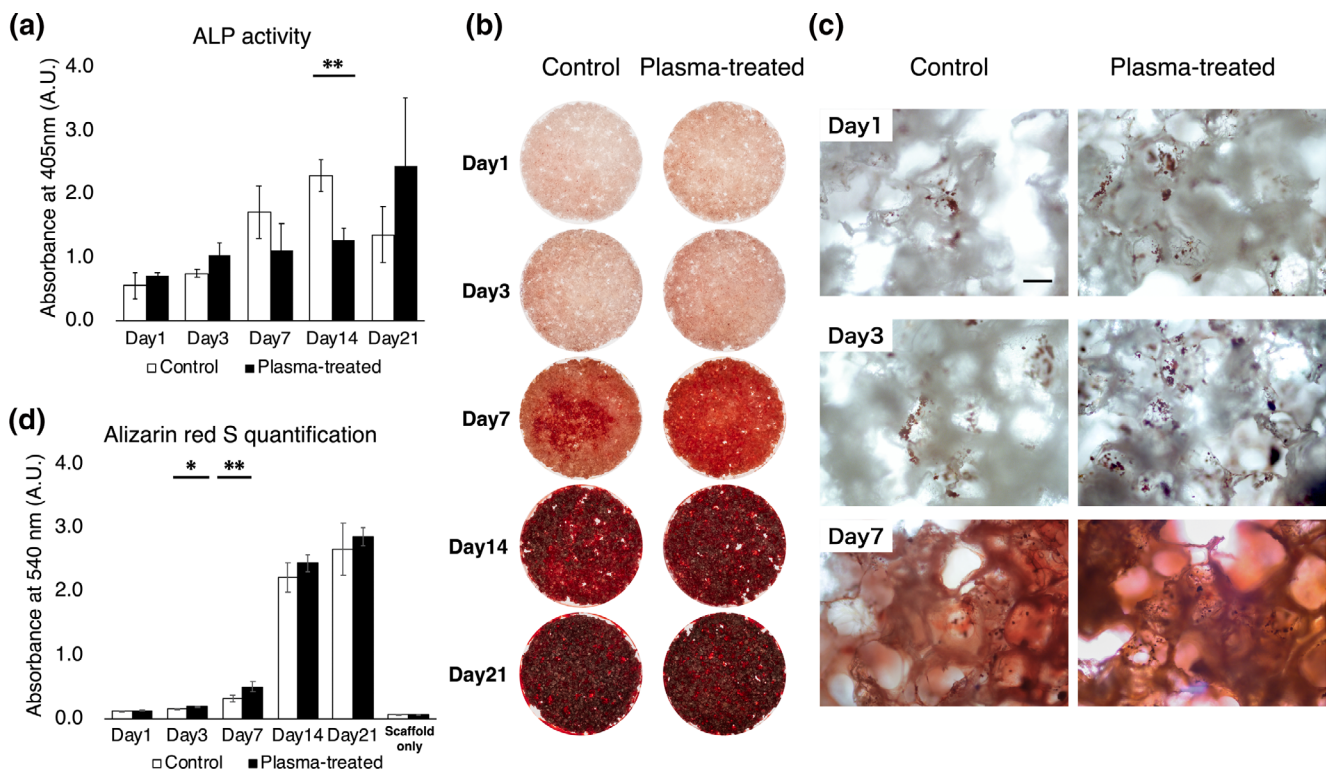
FIGURE 7 Alkaline phosphatase (ALP) activity of bone marrow stem cells and mineralization on the 3D plasma-treated scaffolds for 3 min. (a) ALP activity of bone marrow stem cells on the 3D plasma-treated scaffolds on day 1, 3, 7, 14, and 21 after seeding. (b) Macroscopic and (c) microscopic images of the 3D plasma-treated scaffolds stained with Alizarin Red S. Scale bar = 100 μm (d) The quantification of Alizarin red S staining. Values are presented as mean ± *SEM*. *$p < .05$, **$p < .01$

4 | DISCUSSION

Biodegradable aliphatic polymers such as PLA, PCL, and lactide-TMC, have been tested for various applications in biomedicine and shown to possess decent properties for bone tissue engineering, that is, they are biocompatible and biodegradable and have appropriate mechanical strength as a graft material. They also have good moldability, which allows one to form the materials in arbitrary shapes with high porosity by freeze-drying, salt leaching, gas foaming and 3D printing techniques.[35] In this study, we have selected Lactide-TMC as a scaffold material because Lactide-TMC has higher flexibility than conventional aliphatic polymers such as PLA and PCL, which facilitates handling, fabrication and shaping of the scaffolds.[36] Further, the material is known to possess a unique degradation property. During degradation, the material produces less acidic by-products because of its component, trimethylene carbonate, causing less local inflammation at the implanted sites.[37] However, the hydrophobicity of aliphatic polymers including Lactide-TMC is a common obstacle regardless of the type of applications, hindering efficient cell adhesion and growth, and therefore, a surface modification is preferred.[38]

Plasma as an ionized gas was first described in 1927 by the Nobel laureate Irving Langmuir. Since then, surface treatment by plasma activation has been extensively studied. The first application of plasma for surface modification of biodegradable aliphatic polymers was in 1997, which applied vacuum oxygen and nitrogen plasma to PLA fabrics.[39] Afterward, the treatment has been tested with a variety of cell types, and high biocompatibility has been verified. It is currently applied to biomaterials and biomedical devices approved for clinical implantation.[40] There are several advantages to surface activation of biomaterials with oxygen plasma beyond biocompatibility. Typically, surface oxidation for hydrophilization occurs only within a depth of 5–50 nm from the surface, indicating that plasma activation does not alter the bulk properties of the materials.[41,42] Therefore, the materials can maintain their mechanical properties such as strength, flexibility, formability, stability/degradability while the surfaces are modified to be more bioactive.[18] Further, the fact that oxygen gas is abundant equates to high availability and low cost, which is critical for clinical application.

Our structural and chemical characterization of plasma-treated lactide-TMC is consistent with previous studies using other types of biopolymers. Since wettability is closely influenced by surface chemistry and topography, we have performed SEM and ATR-FTIR together with contact angle measurement. We showed that plasma activation for as short as 1 min significantly increased surface roughness while the addition of functional groups was limited, indicating that changes in surface properties of lactide-TMC after short-term oxygen plasma treatment was mainly due to a mechanical etching effect by bombardment of oxygen molecules rather than chemical modification. We also performed atomic force microscopy (AFM), but we could not obtain reliable data because of extremely rough and inhomogeneous surfaces after the treatment (data not shown). The induced hydrophilicity lasted for at least 2 weeks, which would adapt readily to clinical settings.

Optimal cell adhesion and elongation can only be achieved when the surface wettability is appropriate, which may vary depending on the type of cells as well as materials.[43] Therefore, we first compared cell kinetics on 1, 3, and 5 min-treated surfaces of lactide-TMC with the control surface. On the plasma treated surfaces, initial cell adhesion and elongation of rBMSC were greatly enhanced within 24 hr of seeding in a dose-dependent manner. Moreover, we observed an increase in F-actin intensity on plasma-treated surfaces. The density of F-actin is known to be associated with the strength of cell adhesion as well as the generation of physical forces to change cell morphology and to migrate.[44-46] Recent morphological analyses using adipose-derived MSC revealed the detailed mechanism of accelerated initial cell adhesion on plasma-treated polystyrene surfaces. The cells on plasma-treated surfaces by ammonia, carbon dioxide, and acrylic acid plasma exhibited more filopodia-like and lamellipodial-like protrusions after only 1 hr of adhesion.[20] A promising mechanism for enhancing adhesion was suggested by Griffin et al. They functionalized nanocomposite polymer, POSS-PCU, using different types of plasma gas and showed an increase in total protein absorption to the surface following incubation with serum. This included cell adhesion serum proteins such as fibronectin and vitronectin, suggesting that the surface was modified to be more bioactive.[47] These results together confirm that hydrophilized polymeric surfaces by plasma activation activates cell kinetics.

Further evaluation was conducted with 3D microporous scaffolds as it is crucial to evaluate cell fate in a 3D environment similar to that in vivo. As wettability increased, the seeding efficiency was improved. This was attributed to the high infiltration of cells. The efficiency of cell seeding is a key factor for clinical application because it is directly linked to time and cost of treatment.[48] However, we also showed that the group treated for 5 min had significantly decreased cellular viability, implying that prolonged treatment may affect cell health. Similar findings were reported previously, showing that excessive plasma treatment led to low viability of osteoblast precursors and significantly disrupted cell adhesion.[27] One possible reason could be due to reactive oxygen species (ROS) that are bound to the surface, causing cell senescence and apoptosis,[49-53] and/or simply wettability inappropriate for osteoprogenitors.[54] Therefore, we used 3 min-treated samples for further studies because this increased seeding efficiency equivalent to that seen after 5 min treatment without the risk of compromising cell viability.

Stem cell fate is firmly governed by surface physical properties such as surface roughness, polarity and wettability, which together control the gene expression of uncommitted cells.[55,56] Therefore, we evaluated osteogenesis in an osteoinductive environment. Firstly, the proliferative activity of rBMSC was assessed as it reflects not only cell growth but also osteogenic maturation. The quantification of dsDNA indicates that rBMSC increased their proliferative activity before reaching confluence. Then, the proliferation was suppressed because of tight cell-to-cell contact, which is a prerequisite for osteogenic maturation.[48,57] This process was significantly accelerated in the plasma-treated group. Immunofluorescence of PCNA further demonstrated active cell cycle in both groups by day 7 but the expression gradually

decreased afterwards. Although statistical analysis showed no significance, the intensity as well as the ratio of PCNA+ cells in the plasma-treated group were higher on day 1 and day 3 and lower on day 7 and later. The magnitude of PCNA expression is related to the cell cycle. Cells highly express PCNA during S/G2/M phases and weakly during G1 phase, but cells which do not undergo cell cycle (i.e., G0 phase) do not express PCNA.[58,59] Therefore, our results suggest that the proliferative activity of rBMSC in 3D plasma-treated scaffolds was initially promoted as it was with 2D surfaces, and they commenced their maturation process slightly earlier than the cells on the control surfaces.

RUNX2 is a key transcription factor that plays a major role in driving osteogenic differentiation of precursor cells. In murine osteogenic cells, an initial increase in RUNX2 expression is involved in the induction of differentiation although continuous upregulation is observed.[60,61] We showed that RUNX2 expression was significantly upregulated in mRNA and protein levels in the plasma-treated group on day 7 compared with the control, and the mRNA expression had plateaued by day 14 when the control group showed the highest expression. This indicates that plasma-treated scaffolds accelerated the induction of osteogenic differentiation. Interestingly, despite high mRNA expression, RUNX2 protein accumulated in nuclei was clearly observed only on day 7 and day 14, suggesting there is a discordance between transcription and translation in murine RUNX2. Osterix is the other key osteogenic transcription factor and the downstream target of RUNX2, which is necessary to transform osteogenic precursors into mature osteoblasts.[62] We showed that mRNA expression of osterix was continuously upregulated over the period of differentiation, and that expression was significantly higher in the plasma-treated group throughout the experimental period. The maturation process was confirmed by the expression of BSP and OCN as mature osteoblast markers.[33] Both expression levels were significantly upregulated on day 21 in the plasma-treated group. These findings are consistent with a previous report using an osteoblastic cell line on plasma-treated chitosan scaffolds.[43] However, we were unable to show a clear separation of ALP expression and its activity pattern between the groups. A possible mechanism of increased expression in the late phase, based on previous findings, is that the release of plasma membrane vesicles is a part of a controlled apoptosis process, which is necessary for tissue-specific maturation.[63-65] This was also demonstrated with osteoblastic cells in which the release of ALP from osteoblastic cells undergoing apoptosis was involved in mineralisation.[66] Additionally, ALP is involved in numerous biological processes, and it is expressed in all of living cells.[67] Collagen type 1 is the main extracellular matrix in bone. RT-qPCR showed that Col1A1a expression was significantly higher in the plasma-treated group on day 3, but the trend was reversed on day 7. This is supported by immunofluorescence showing that the formation of collagen type 1 was established as early as on day 7 on the plasma-treated scaffolds. Apart from the increase in collagen formation activity of rBMSC, previous studies have found that wettability itself alters the assembly pattern of collagen fibers, which further activates cell-matrix interaction via integrin α1 and α2

heterodimers.[68,69] This suggests not only that modified surface properties enhance collagen formation by the cells but also that collagen matrix formed on the treated surface further enhance cell activity. Finally, the promotion of osteogenic differentiation was confirmed by alizarin red S staining, showing more calcium deposition in the plasma-treated group, particularly on day 3 and day 7. It is noteworthy that non-uniformity of staining was observed in the control. This is probably ascribed to inhomogeneous cell seeding because of hydrophobicity of the untreated material. Although it appears the control group caught up with the plasma-treated group on day 21 in terms of mineralization and collagen formation, this is probably due to supersaturation of the formed substances. Thus, the promotion of osteogenic differentiation may persist longer than 21 days.

In this study, we have chosen oxygen plasma mainly because of high availability and cost-effectiveness. Additionally, it can also hydroxylate and etch the polymer surfaces, which is ideal for the purpose of hydrophilisation.[48,70] However, different types of plasma cause diverse surface chemistry and topography, leading to different biological effects.[71] It has been reported that plasma activation with argon gas but not oxygen gas promoted chondrogenic and osteogenic differentiation of rat adipose-derived stem cells.[72] Hence, the ideal plasma gas and dosage should be optimized for each cell type, species and therapeutic target tissue.

5 | CONCLUSION

In this work, the surface of flat films and 3D microporous scaffolds of the aliphatic polymer lactide-TMC was modified by oxygen plasma for different treatment times (i.e., 1, 3, and 5 min). After treatment, nanotopographical roughness of lactide-TMC significantly increased, resulting in improved wettability. Importantly, the effect persisted at least for 2 weeks after treatment, which may potentially facilitate the translation of plasma-treated polymeric scaffolds to the clinical setting. We found that initial cell adhesion and elongation of rBMSC on plasma-treated surfaces were significantly promoted compared to the control. Also, a higher seeding efficiency was achieved when scaffolds were treated for more than 3 min. However, prolonged treatment was associated with lower cell viability, and therefore, 3 min-treatment was considered optimal for the evaluation of osteogenesis of rBMSC. We showed that cell growth and osteogenic differentiation were significantly promoted in the plasma-treated group, resulting in the promotion of extracellular matrix formation and mineral deposition. Surface activation with oxygen plasma is a promising strategy for bone tissue engineering as it is an accessible technique that can modify surface properties suitable for cell growth and osteogenic differentiation without compromising the bulk properties.

CONFLICT OF INTEREST

The authors declare no potential conflict of interest.

DATA AVAILABILITY STATEMENT

The data that support the findings of this study are available from the corresponding author upon reasonable request.

ORCID

*Shuntaro Yamada* https://orcid.org/0000-0003-0282-5498

REFERENCES

1. Campana V, Milano G, Pagano E, et al. Bone substitutes in orthopaedic surgery: from basic science to clinical practice. *J Mater Sci Mater Med*. 2014;*25*:2445-2461.
2. Roddy E, DeBaun MR, Daoud-Gray A, Yang YP, Gardner MJ. Treatment of critical-sized bone defects: clinical and tissue engineering perspectives. *Eur J Orthop Surg Traumatol*. 2018;*28*:351-362.
3. Amini AR, Laurencin CT, Nukavarapu SP. Bone tissue engineering: recent advances and challenges. *Crit Rev Biomed Eng*. 2012;*40*: 363-408.
4. Fuoco T, Mathisen T, Finne-Wistrand A. Poly(l-lactide) and poly(l-lactide-co-trimethylene carbonate) melt-spun fibers- structure–processing–properties relationship. *Biomacromolecules*. 2019;*20*: 1346-1361.
5. Guo GK, Lu ZQ, Zhang Y, Li SM. In vivo study on the histocompatibility and degradation behavior of biodegradable. *Acta Biochim Biophys Hung*. 2011;*43*:433.
6. Messias AD, Martins KF, Motta AC, Duek EA, Synthesis d R. Characterization, and osteoblastic cell culture of poly(L-co-D,L-lactide-co-trimethylene carbonate) scaffolds. *Int J Biomater*. 2014;*2014*:1-7.
7. Ji L-J, Lai K-L, He B, et al. Study on poly(l-lactide-co-trimethylene carbonate): synthesis and cell compatibility of electrospun film. *Biomed Mater*. 2010;*5*:045009.
8. Hassan MN, Yassin MA, Suliman S, Lie SA, Gjengedal H, Mustafa K. The bone regeneration capacity of 3D-printed templates in calvarial defect models: a systematic review and meta-analysis. *Acta Biomater*. 2019;*91*:1-23.
9. Sisson AL, Ekinci D, Lendlein A. The contemporary role of ε-caprolactone chemistry to create advanced polymer architectures. *Polymer*. 2013;*54*:4333-4350.
10. Jamshidian M, Tehrany EA, Imran M, Jacquot M, Desobry S. Polylactic acid: production, applications, nanocomposites, and release studies. *Compr Rev Food Sci Food Saf*. 2010;*9*:552-571.
11. Jeon H, Lee H, Kim GA. Surface-modified poly(ε-caprolactone) scaffold comprising variable nanosized surface-roughness using a plasma treatment. *Tissue Eng Part C Method*. 2014;*20*:951-963.
12. Kim K, Dean D, Mikos AG, Fisher JP. Effect of initial cell seeding density on early osteogenic signal expression of rat bone marrow stromal cells cultured on cross-linked poly(propylene fumarate) disks. *Biomacromolecules*. 2009;*10*:1810-1817.
13. Francis K, Palsson BO. Effective intercellular communication distances are determined by the relative time constants for cytochemokine secretion and diffusion (cell signalingbioreactor designtissue engineering). 1997;*94*:12258.
14. Mauck RL, Wang CCB, Oswald ES, Ateshian GA, Hung CT. The role of cell seeding density and nutrient supply for articular cartilage tissue engineering with deformational loading. *Osteoarthritis Cartilage*. 2003; *11*:879-890.
15. Lane SW, Williams DA, Watt FM. Modulating the stem cell niche for tissue regeneration. *Nat Biotechnol*. 2014;*32*:795-803.
16. Schofield R. The relationship between the spleen colony-forming cell and the haemopoietic stem cell. *Blood Cells*. 1978;*4*(1-2):7-25.
17. Recek N, Resnik M, Motaln H, et al. Cell adhesion on poly-caprolactone modified by plasma treatment. *Int J Polym Sci*. 2016; *2016*:1-9.
18. Jacobs T, Morent R, De Geyter N, Dubruel P, Leys C. Plasma surface modification of biomedical polymers: influence on cell-material interaction. *Plasma Chem Plasma Process*. 2012;*32*:1039-1073.
19. Qiu Z-Y, Chen C, Wang X-M, Lee I-S. Advances in the surface modification techniques of bone-related implants for last 10 years. *Regen Biomater*. 2014;*1*:67-79.
20. Kleinhans C, Schmohl L, Barz J, Kluger PJ. Low-pressure plasma activation enables enhanced adipose-derived stem cell adhesion. *J Biomed Mater Res - Part B Appl Biomater*. 2020;*108*(4):1527-1535.
21. Li Y, Kim JH, Choi EH, Han I. Promotion of osteogenic differentiation by non-thermal biocompatible plasma treated chitosan scaffold. *Sci Rep*. 2019;*9*:3712.
22. Barradas AMC, Lachmann K, Hlawacek G, et al. Surface modifications by gas plasma control osteogenic differentiation of MC3T3-E1 cells. *Acta Biomater*. 2012;*8*:2969-2977.
23. Trappmann B, Gautrot JE, Connelly JT, et al. Extracellular-matrix tethering regulates stem-cell fate. *Nat Mater Nature*. 2012;*11*:642-649.
24. Park JH, Wasilewski CE, Almodovar N, et al. The responses to surface wettability gradients induced by chitosan nanofilms on microtextured titanium mediated by specific integrin receptors. *Biomaterials*. 2012; *33*:7386-7393.
25. Hao L, Fu X, Li T, et al. Surface chemistry from wettability and charge for the control of mesenchymal stem cell fate through self-assembled monolayers. *Colloids Surf B Biointerfaces*. 2016;*148*:549-556.
26. Zhang T, Lin S, Shao X, et al. Effect of matrix stiffness on osteoblast functionalization. *Cell Prolif*. 2017;*50*:e12338.
27. Olivares-Navarrete R, Hyzy SL, Hutton DL, et al. Role of non-canonical Wnt signaling in osteoblast maturation on microstructured titanium surfaces. *Acta Biomater*. 2011;*7*:2740-2750.
28. Galli C, Piemontese M, Lumetti S, Manfredi E, MacAluso GM, Passeri G. The importance of WNT pathways for bone metabolism and their regulation by implant topography. *Eur Cell Mater*. 2012;*24*:46-59.
29. Odelius K, Plikk P, Albertsson A-C. Elastomeric hydrolyzable porous scaffolds: copolymers of aliphatic polyesters and a polyether-ester. *Biomacromolecules*. 2005;*6*:2718-2725.
30. Yassin MA, Leknes KN, Pedersen TO, et al. Cell seeding density is a critical determinant for copolymer scaffolds-induced bone regeneration. *J Biomed Mater Res Part A*. 2015;*103*:3649-3658.
31. Schindelin J, Arganda-Carreras I, Frise E, et al. Fiji: an open source platform for biological image analysis. *Nat Methods*. 2012;*9*:676-682.
32. Livak KJ, Schmittgen TD. Analysis of relative gene expression data using real-time quantitative PCR and the 2(-Delta Delta C[T]) method. *Methods*. 2001;*25*:402-408.
33. Miron RJ, Zhang YF. Osteoinduction: a review of old concepts with new standards. *J Dent Res*. 2012;*91*:736-744.
34. Suto EG, Mabuchi Y, Suzuki N, et al. Prospectively isolated mesenchymal stem/stromal cells are enriched in the CD73+ population and exhibit efficacy after transplantation. *Sci Rep*. 2017;*7*(4838):1-10.
35. Pina S, Ribeiro VP, Marques CF, et al. Scaffolding strategies for tissue engineering and regenerative medicine applications. *Materials*. 2019; *12*:1824.
36. Sartoneva R, Nordback PH, Haimi S, et al. Comparison of poly(l-lactide-co-ε-caprolactone) and poly(trimethylene carbonate) membranes for urethral regeneration: an in vitro and in vivo study. *Tissue Eng Part A*. 2018;*24*(1-2):117-127.
37. Fukushima K. Poly(trimethylene carbonate)-based polymers engineered for biodegradable functional biomaterials. *Biomater Sci*. 2016;*4*(1): 9-24.
38. Yassin MA, Leknes KN, Sun Y, Lie SA, Finne-Wistrand A, Mustafa K. Surfactant tuning of hydrophilicity of porous degradable copolymer scaffolds promotes cellular proliferation and enhances bone formation. *J Biomed Mater Res Part A*. 2016;*104*:2049-2059.

39. Hirotsu T, Masuda T, Matumura Y, Takahashi M. Surface effects of plasma treatments on some biodegradable polymers. *J Photopolym Sci Technol*. 1997;10:123-128.

40. Bose S, Robertson SF, Bandyopadhyay A. Surface modification of biomaterials and biomedical devices using additive manufacturing. *Acta Biomater*. 2018;66:6-22.

41. Altuncu E, Üstel F, Esen SG, Karayel E. Infuence of oxygen and nitrogen plasma treatment on polypropyleme (PP) bumper surface. *J Achiev Mater Manuf Eng*. 2016;77:18.

42. Lin W-C, Mohd Razali N. Temporary wettability tuning of PCL/PDMS micro pattern using the plasma treatments. *Materials*. 2019;12:644.

43. Dowling DP, Miller IS, Ardhaoui M, Gallagher WM. Effect of surface wettability and topography on the adhesion of osteosarcoma cells on plasma-modified polystyrene. *J Biomater Appl*. 2011;26:327-347.

44. Gardel ML, Schneider IC, Aratyn-Schaus Y, Waterman CM. Mechanical integration of actin and adhesion dynamics in cell migration. *Annu Rev Cell Dev Biol*. 2010;26:315-333.

45. Kwon S, Yang W, Moon D, Kim KS. Biomarkers to quantify cell migration characteristics. *Cancer Cell Int BioMed Central*. 2020;20:1.

46. Dogterom M, Koenderink GH. Actin-microtubule crosstalk in cell biology. *Nat Rev Mol Cell Biol*. 2019;20:38-54.

47. Griffin MF, Ibrahim A, Seifalian AM, Butler PEM, Kalaskar DM, Ferretti P. Chemical group-dependent plasma polymerisation preferentially directs adipose stem cell differentiation towards osteogenic or chondrogenic lineages. *Acta Biomater*. 2017;50:450-461.

48. Hettle R, Corbett M, Hinde S, et al. The assessment and appraisal of regenerative medicines and cell therapy products: an exploration of methods for review, economic evaluation and appraisal. *Health Technol Assess*. 2017;21:1-204.

49. Jha N, Ryu JJ, Choi EH, Kaushik NK. Generation and role of reactive oxygen and nitrogen species induced by plasma, lasers, chemical agents, and other systems in dentistry. *Oxid Med Cell Longev*. 2017;2017:1-13.

50. Arndt S, Wacker E, Li Y-F, et al. Cold atmospheric plasma, a new strategy to induce senescence in melanoma cells. *Exp Dermatol*. 2013;22:284-289.

51. Weiss M, Gümbel D, Hanschmann E-M, et al. Cold atmospheric plasma treatment induces anti-proliferative effects in prostate cancer cells by redox and apoptotic signaling pathways. *PLoS One*. 2015;10:e0130350.

52. Xia J, Zeng W, Xia Y, et al. Cold atmospheric plasma induces apoptosis of melanoma cells via sestrin2-mediated nitric oxide synthase signaling. *J Biophotonics*. 2019;12:e201800046.

53. Turrini E, Laurita R, Stancampiano A, et al. Cold atmospheric plasma induces apoptosis and oxidative stress pathway regulation in T-lymphoblastoid leukemia cells. *Oxid Med Cell Longev*. 2017;2017:1-13.

54. Hao L, Yang H, Du C, et al. Directing the fate of human and mouse mesenchymal stem cells by hydroxyl–methyl mixed self-assembled monolayers with varying wettability. *J Mater Chem B*. 2014;2:4794-4801.

55. Oehr C. Plasma surface modification of polymers for biomedical use. *Nucl Instru Method Phys Res Sec B Beam Interact Mater Atoms*. 2003;208:40.

56. Ferrari M, Cirisano F, Morán MC. Mammalian cell behavior on hydrophobic substrates: influence of surface properties. *Colloids Interf*. 2019;3:48.

57. Abo-Aziza FAM, Az A. The impact of confluence on bone marrow mesenchymal stem (BMMSC) proliferation and osteogenic differentiation. *Int J Hematol Stem Cell Res*. 2017;11:121.

58. Zerjatke T, Gak IA, Kirova D, et al. Quantitative cell cycle analysis based on an endogenous all-in-one reporter for cell tracking and classification. *Cell Rep*. 2017;19:1953-1966.

59. Schönenberger F, Deutzmann A, Ferrando-May E, Merhof D. Discrimination of cell cycle phases in PCNA-immunolabeled cells. *BMC Bioinformatics*. 2015;16:180.

60. Liu B, Lu Y, Wang Y, Ge L, Zhai N, Han J. A protocol for isolation and identification and comparative characterization of primary osteoblasts from mouse and rat calvaria. *Cell Tissue Bank*. 2019;20:173-182.

61. Hassumi JS, Mulinari-Santos G, Fabris AL d S, et al. Alveolar bone healing in rats: micro-CT, immunohistochemical and molecular analysis. *J Appl Oral Sci*. 2018;26:e20170326.

62. Hojo H, Ohba S, He X, Lai LP, McMahon AP. Sp7/osterix is restricted to bone-forming vertebrates where it acts as a dlx co-factor in osteoblast specification. *Dev Cell*. 2016;37:238-253.

63. Huppertz B, Frank HG, Kaufmann P. The apoptosis cascade-morphological and immunohistochemical methods for its visualization. *Anat Embryol*. 1999;200:1-18.

64. Mills JC, Stone NL, Pittman RN. Extranuclear Apoptosis. *J Cell Biol*. 1999;146:703-708.

65. Johansson A-C, Appelqvist H, Nilsson C, Kågedal K, Roberg K, Öllinger K. Regulation of apoptosis-associated lysosomal membrane permeabilization. *Apoptosis*. 2010;15:527-540.

66. Farley JR, Stilt-Coffing B. Apoptosis may determine the release of skeletal alkaline phosphatase activity from human osteoblast-line cells. *Calcif Tissue Int*. 2001;68:43-52.

67. Štefková K, Procházková J, Pacherník J. Alkaline phosphatase in stem cells. *Stem Cells Int*. 2015;1:2015.

68. Coelho NM, González-García C, Planell JA, Salmerón-Sánchez M, Altankov G. Different assembly of type IV collagen on hydrophilic and hydrophobic substrata alters endothelial cells interaction. *Eur Cell Mater*. 2010;19:262-272.

69. Coelho NM, González-García C, Salmerón-Sánchez M, Altankov G. Arrangement of type IV collagen on NH2 and COOH functionalized surfaces. *Biotechnol Bioeng*. 2011;108:3009-3018.

70. Yamamoto M, Matsumae T, Kurashima Y, et al. Comparison of argon and oxygen plasma treatments for ambient room-temperature wafer-scale au–au bonding using ultrathin au films. *Micromachines*. 2019;10:119.

71. Griffin M, Palgrave R, Baldovino-Medrano V, Butler P, Kalaskar D. Argon plasma improves the tissue integration and angiogenesis of subcutaneous implants by modifying surface chemistry and topography. *Int J Nanomedicine*. 2018;13:6123-6141.

72. Griffin MF, Ibrahim A, Seifalian AM, Butler PEM, Kalaskar DM, Ferretti P. Argon plasma modification promotes adipose derived stem cells osteogenic and chondrogenic differentiation on nanocomposite polyurethane scaffolds; implications for skeletal tissue engineering. *Mater Sci Eng C*. 2019;105:110085.
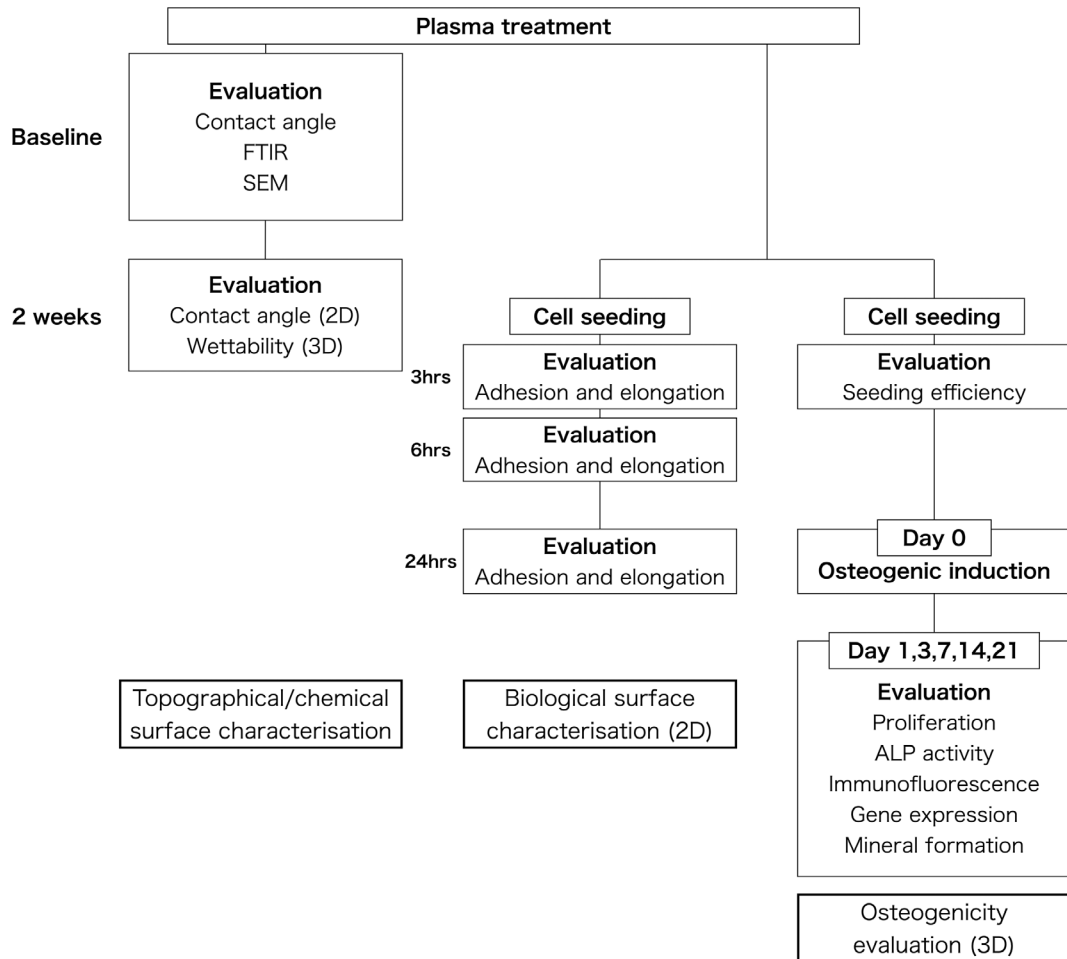
APPENDIX
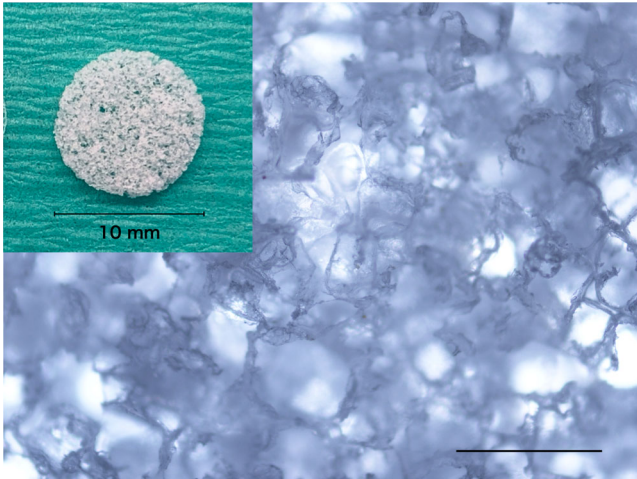
FIGURE A1 Macro- and microscopic image of lactide-TMC microporous scaffolds used in the study. Scale bar = 500 μm (microscopic image)

FIGURE A2 Experimental flow and timeline